Kovove Mater. 64 2026 107–117
DOI: 10.31577/km.2026.2.107

Numerical investigation of stress ratio and geometry effects on fatigue behavior of 2024-T3 aluminum alloy

Ahmet Murat Asan[1]*

[1] *Machine Program, Department of Machine and Metal Technologies, Organized Industrial Zone Vocational School, Mardin Artuklu University, Mardin, Turkey*

Received 29 January 2026, received in revised form 24 March 2026, accepted 19 May 2026

Abstract

The fatigue performance of 2024-T3 aluminum alloy is of critical importance in aerospace applications, yet the combined effects of stress ratio and geometry remain insufficiently explored. The objective of this study is to numerically investigate how different stress ratios (R = –0.2, 0.1, 0.4) and specimen geometries influence fatigue life, damage, and safety factor under varying tensile stresses (483, 241.5, and 120.75 MPa). Three specimen configurations – open-hole, transverse, and shear – were modeled and simulated using ANSYS Workbench, with input data obtained from literature-based mechanical properties and S-N curves. Results demonstrate that increasing tensile stress markedly reduces fatigue life and safety factor, whereas stress ratio exerts a non-linear influence, with intermediate values yielding the most detrimental effect. The findings reveal the interaction between stress ratio and geometry, providing new insights for fatigue life prediction and structural design of 2024-T3 aluminum alloy.

K e y w o r d s: fatigue life, stress ratio, 2024-T3 aluminum alloy, finite element analysis, specimen geometry, S-N curve

1. Introduction

2024 aluminum alloy (2024-T3), a member of the hard aluminum group, is extensively employed in aerospace applications such as fuselage skins, wing ribs, and various structural components [1–3]. Its widespread utilization arises from favorable properties including good machinability, excellent formability, and superior resistance to fatigue [4]. Statistical data indicate that fatigue failure is a major concern for structural elements in aircraft, representing a significant safety challenge in the aviation industry. Many aircraft accidents have been directly attributed to fatigue damage in structural parts, highlighting the critical need for fatigue assessment [5–7]. The occurrence of fatigue cracks in aluminum alloy components during service can lead to catastrophic consequences, including severe accidents and even loss of human life. Therefore, ensuring the durability and reliability of aluminum alloy structures under cyclic loading is essential for the aerospace sector. Previous studies on the fatigue behavior of aluminum alloys can be broadly classified into experimental, numerical, and repair-based approaches. In particular, numerical approaches such as finite element methods and XFEM have gained significant attention for predicting fatigue life and crack propagation behavior. When the studies on the fatigue behavior of aluminum alloys are examined in the literature, Fageehi [8] numerically investigated the fatigue life of a perforated plate made of Aluminum 7075-T6 alloy (7075-T6) and reported that the presence of the hole significantly affects the fatigue life. Li et al. [9] proposed a new continuous failure mechanics-based model to predict the thermal corrosion fatigue life of Al alloys, validating their model with experimental data. Gairola et al. [10] applied the extended finite element method (XFEM) to analyze the fatigue behavior of Al 2024. Nejad et al. [11] experimentally determined the fatigue life of riveted joints in 2024-T3 sheets and reported that the fatigue life increases with increasing rivet shank length and rivet diameter. The fatigue behavior of specimens prepared using two V-notch cracked Al alloys (2024-T3 and 7075-T6) repaired with carbon/epoxy patches was

*Corresponding author: e-mail address: ahmetmuratasan@artuklu.edu.tr

T a b l e 1. Mechanical properties of material [32]

Material	Elastic modulus, E (GPa)	Poisson ratio, v	Shear modulus, G (GPa)
2024-T3	71.6	0.33	26.9

investigated experimentally and numerically by Mohammed et al. [12], who concluded that rectangular-shaped patches were more efficient than triangular and trapezoidal ones. Chen et al. [13] examined the fatigue crack propagation behavior of 2024 aluminum alloy under varying stress ratios ($R = 0.1$, 0.2, 0.4). Dai et al. [14, 15] also applied the MAO coating method to 2024-T3 and 7075-T6 alloys and experimentally determined the fatigue behavior under different duty cycles. Borges et al. [16] studied the variation of fatigue crack growth (FCG) of AA2024-T351 (2024-T351) with increasing stress ratio ($R = 0.1$–0.7) and reported that the FCG rate increases as R increases. Yadav et al. [17] investigated the influence of a 3.5% NaCl solution on the fatigue crack behavior of welded 2024-T3 and concluded that exposure to the solution reduces fatigue life. Other investigations include Nejad et al. [18, 19], who analyzed riveted joints in 2024-T3 sheets both numerically and experimentally, and Chakherlou et al. [20], who examined fretting fatigue in cold-expanded plates. Duncheva et al. [21] investigated the effect of single toroidal roller burnishing on 2024-T3 and reported an increase in fatigue limit. Maximov et al. [22] proposed a method to enhance fatigue life in fastener holes of 2024-T3. Although some studies focused on different materials such as 7075 aluminum alloys and GLARE laminates, these works provide general insights into fatigue mechanisms. Gao et al. [23] experimentally investigated the fatigue behavior of notched glass fiber reinforced aluminum (GLARE) sheets. Madhavi et al. [24] examined the fatigue behavior of AA6061-T6 (6061-T6) coated with micro-arc oxidation (MAO) at different thicknesses and reported that 50 μm is the optimum coating thickness. Ganesan et al. [25] compared the fatigue life of welded and non-welded AA7075-T651 (7075-T651) joints and concluded that welding improves fatigue life. Zhang et al. [26] investigated the influence of ultrasonic nanocrystalline surface modification (UNSM) on corroded 7075-T651 aluminum alloy and reported that UNSM significantly increases fatigue life. You et al. [27] analyzed the effects of friction coefficient and impact angle on GLARE laminates under low--speed impacts using *ABAQUS/Explicit*. Zamani et al. [28] investigated adhesive-bonded Al-GFRP single-lap joints under varying maximum fatigue loads and load ratios. Mosayyebi and Chakherlou [29] studied the effect of composite patch geometry on the fatigue life of V-notch and cracked aluminum panels and validated their numerical results with experimental findings, showing that the use of patches improves fatigue life. Taware et al. [30] numerically studied the fatigue performance of edge-cracked 6061-T6 panels repaired with asymmetric CFRP patches and reported improved fatigue performance. Ahmed et al. [31] investigated the effects of distilled water aging on CFRP patches bonded to 2024-T3 sheets and concluded that the aging effect has a negligible influence on mechanical properties. However, limited studies have systematically investigated the combined effects of stress ratio and specimen geometry on the fatigue behavior of 2024-T3 using numerical methods. This paper numerically investigates the variation of fatigue behavior of 2024-T3 for different stress ratios ($R =$ –0.2, 0.1, and 0.4) and tensile stress levels (483, 241.5, and 120.75 MPa). Three specimen types (open-hole, transverse, and shear) were designed in a CAD environment and imported into ANSYS Workbench in ".step" format. Fatigue simulations were performed using literature-based mechanical properties and S-N curves. Therefore, this study numerically investigates the combined effects of stress ratio and specimen geometry on fatigue life, damage, and safety factor of 2024-T3, revealing the interaction between these parameters and providing a comparative evaluation across different specimen geometries, thereby offering original contributions to the literature.

The paper is structured as follows: Section 2 provides an overview of the alloy and specimen configurations, as well as finite element modeling details. Section 3 presents and discusses the influence of tensile stresses and stress ratios on fatigue life, failure, and safety factor. Section 4 concludes the study.

2. Test method and procedure

2.1. Material and specimen

In this research, 2024-T3 was selected to investigate the effects of stress ratio and stress level on its fatigue performance. The mechanical properties employed in the simulations were obtained from an experimental study reported in the literature [32] and are summarized in Table 1. Three specimen geometries were considered, each prepared in accordance with different ASTM standards. The first configuration was the open-hole specimen (OHS) defined by ASTM D6484 [33], featuring a 6 mm hole, a thickness of 0.1524 mm, a width of 36 mm, and a length

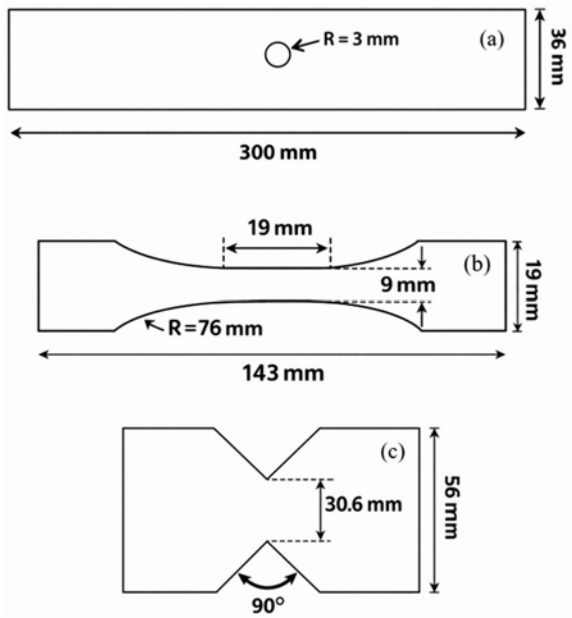

Fig. 1. Dimensions of the specimens: (a) OHS, (b) TS, and (c) SS [33–35].

of 300 mm. The second was the transverse specimen (TS), modeled according to ASTM 638 [34], with a thickness of 0.1524 mm, a width of 19 mm, and a length of 143 mm. The third was the shear specimen (SS) following ASTM 7078 [35], characterized by a thickness of 0.1524 mm, a width of 56 mm, and a length of 76 mm. These three specimen types were selected to systematically investigate the effect of geometry on fatigue behavior, as each type represents different stress concentration and loading conditions encountered in structural components. Moreover, the extent and shape of the plasticity zone resulting from fatigue loading are expected to differ among these specimen types due to variations in stress distribution and constraint conditions. All specimen models were created using CAD software, and their dimensions are presented in Fig. 1.

The modeled specimens were converted to ".step" format and transferred to the *ANSYS Workbench program.* Here, mechanical properties and the S-N curves were defined for the program. The S-N curves were defined separately for each stress ratio ($R = -0.2$, 0.1, and 0.4). The negative stress ratio ($R = -0.2$) was chosen to represent tension–compression loading, where crack closure effects become significant. The small positive ratio ($R = 0.1$) reflects loading conditions commonly encountered in aerospace structures, whereas the higher positive ratio ($R = 0.4$) was used to examine the effect of reduced stress range ($\Delta\sigma$) on fatigue life. The case of $R = 0$ was not considered, since this loading condition, corresponding to a fully tensile but zero-based cycle, is generally regarded

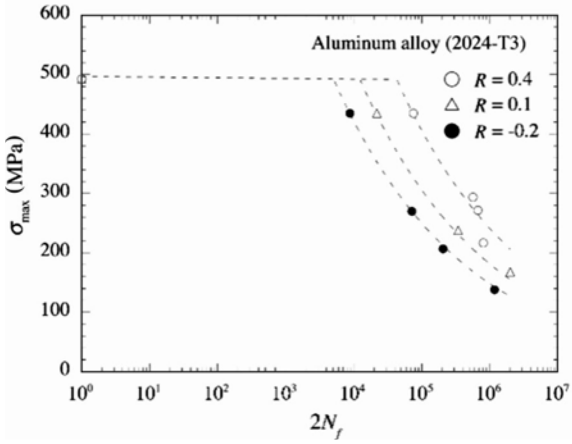

Fig. 2. S-N curves of 2024-T3 [36].

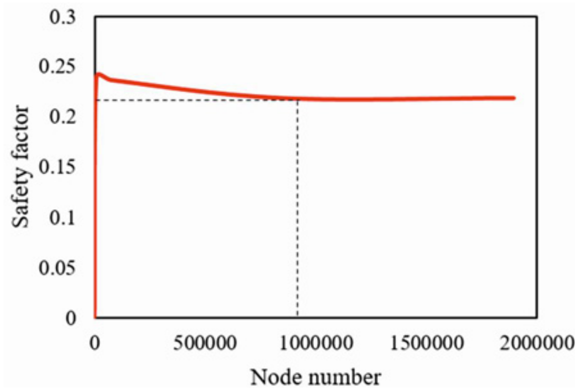

Fig. 3. Mesh convergence analysis for OHS.

in the literature as non-stable fatigue and does not accurately capture crack opening and closure mechanisms observed in practical applications. This S-N curve was obtained from the literature and given in Fig. 2 [36]. Then, the meshing process was carried out. To obtain optimal results, mesh convergence analyses were performed for all specimen types (OHS, TS, and SS). Figure 3 presents the mesh convergence result for the OHS specimen as a representative case. In the convergence plot, once the safety factor value stabilized despite an increase in the number of nodes, the selected mesh size was considered suitable for the analyses. Similar convergence trends were observed for the TS and SS specimens. The finite element models and boundary conditions for different specimen types are presented in Fig. 4. The mesh characteristics of these finite element models are given in Table 2. The OHS specimen has a higher number of elements due to the geometric complexity around the hole, which requires finer mesh discretization. Three-dimensional quadratic SOLID186 elements were employed in the finite element models to ensure accurate representation of stress gradients and fatigue behavior.

Table 2. Mesh characteristics of the finite element models for different specimen types

	Specimen type		
	OHS	TS	SS
Total number of elements	119704	58800	44170
Total number of nodes	843688	414653	311528

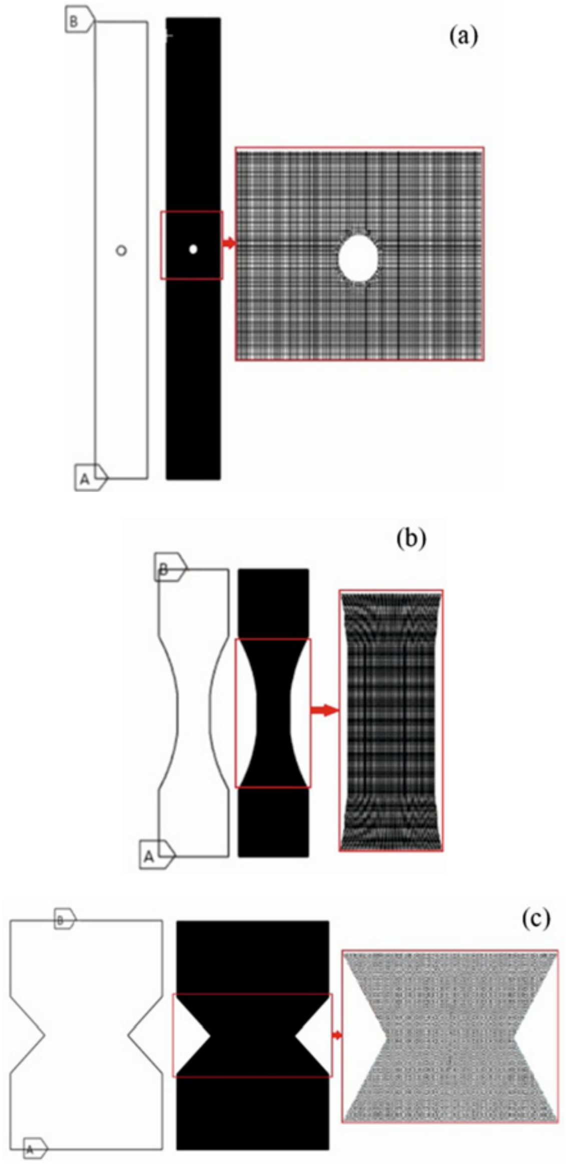

Fig. 4. Finite element models and applied boundary conditions of the specimens: (a) OHS, (b) TS, and (c) SS (A: fixed support, B: applied tensile stress).

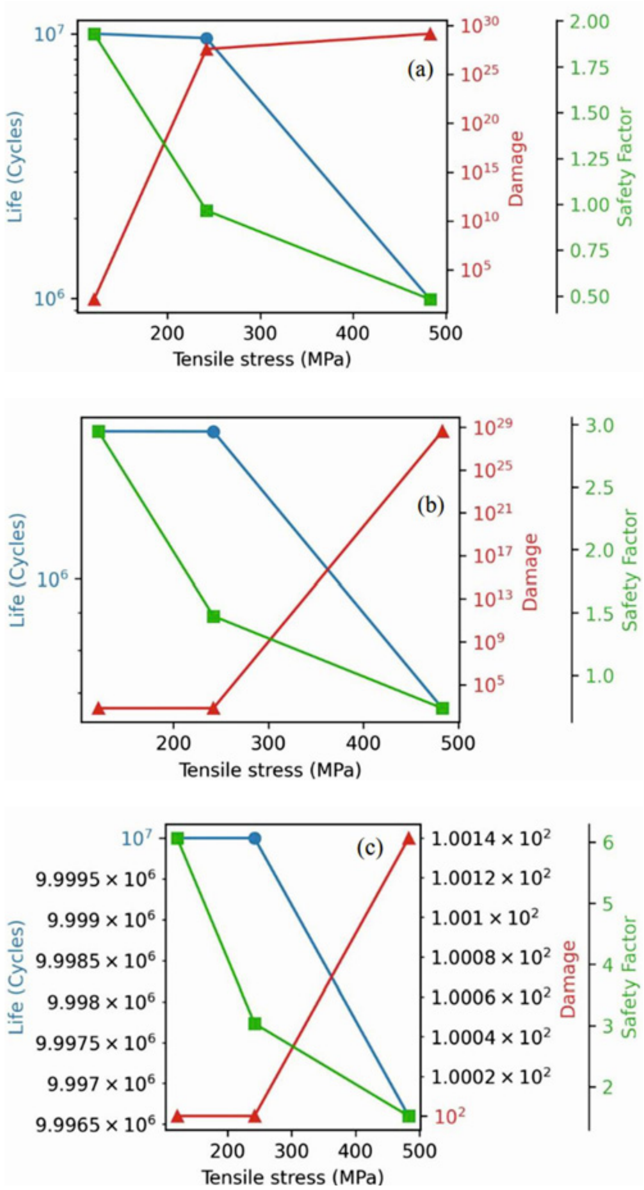

Fig. 5. Variation of parameters for the OHS specimen under different stress ratios: (a) $R = -0.2$, (b) $R = 0.1$, and (c) $R = 0.4$.

3. Results and discussion

In this section, the fatigue behavior of three different specimens is evaluated in terms of their variation with tensile stress (σ) and stress ratio (R). The results presented in the figures represent average values. In addition, deformation results corresponding to fatigue life at $\sigma = 483$, 241.5, and 120.75 MPa are also illustrated.

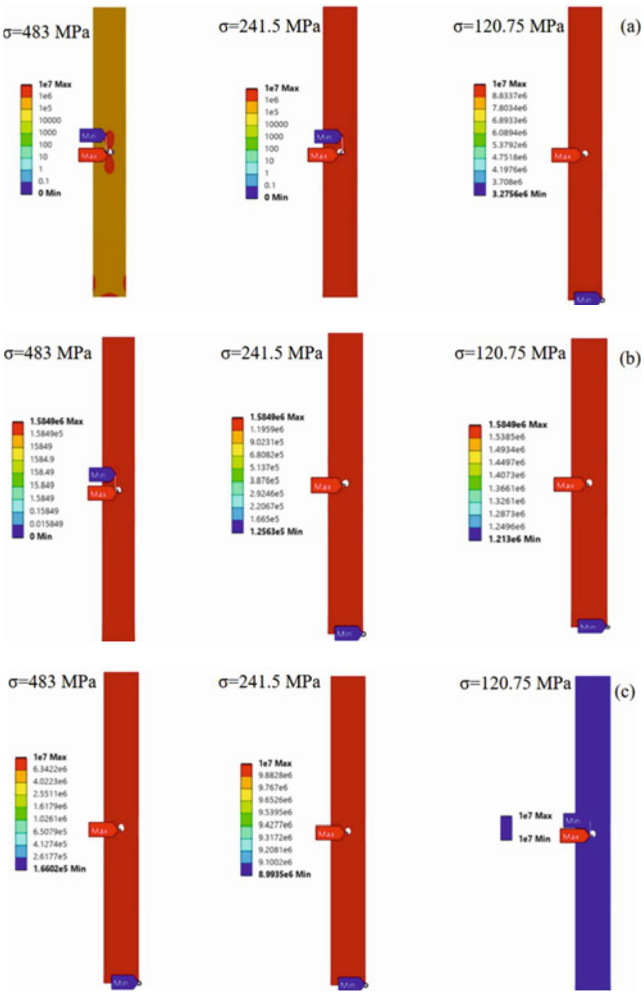

Fig. 6. Variation of deformation for the OHS specimen at different stress ratios: (a) $R = -0.2$, (b) $R = 0.1$, and (c) $R = 0.4$.

3.1. Analysis results for OHS specimen

The variation of fatigue behavior for the OHS specimen is presented in Figs. 5 and 6 in terms of tensile stress (σ) and stress ratio (R). The plotted results in Figs. 5a–c show that fatigue life and safety factor decrease, while damage increases with increasing σ for all stress ratios. This trend can be attributed to the increase in plastic deformation and accelerated microcrack initiation at higher stress levels. Under cyclic loading, crack propagation becomes faster, which significantly reduces the fatigue life of the material. In addition, since the safety factor is defined as the ratio of allowable strength to applied stress, it decreases with increasing σ, indicating a higher risk of failure. For $R = -0.2$, as shown in Fig. 6a, the minimum life regions are highly localized around the hole at $\sigma = 483$ MPa, indicating that fatigue damage initiates in these stress concentration regions. As the applied stress decreases to 241.5 and 120.75 MPa, the distribution of fatigue life becomes more uniform and the minimum life increases significantly. At the lowest stress level, the fatigue life reaches values exceeding 10^6 cycles, indicating a substantial improvement in fatigue resistance. For $R = 0.1$, as illustrated in Fig. 6b, the failure regions become more widespread compared to the $R = -0.2$ case. This indicates that the positive stress ratio promotes earlier and more distributed fatigue damage across the specimen. Although the stress levels are the same, the presence of a positive mean stress accelerates fatigue damage accumulation, leading to a reduction in fatigue life. For $R = 0.4$, as shown in Fig. 6c, the effect of the positive stress ratio becomes more pronounced. While the behavior at higher stress levels is similar to the $R = -0.2$ case, at $\sigma = 120.75$ MPa the fatigue life can be considered effectively infinite, as the minimum cycle exceeds 10^6. The contour plots also indicate that the damage is significantly reduced and distributed more uniformly across the specimen. Overall, for the OHS specimen, both tensile stress and stress ratio play critical roles in fatigue behavior. Increasing σ leads to a sharp reduction in fatigue life, while positive stress ratios promote earlier fatigue initiation and more distributed damage, especially around the hole region where stress concentration is dominant. These results are consistent with previous studies. Mazlan et al. [37] and Liu et al. [38] reported that increasing stress levels accelerate crack initiation and propagation, while Evran [39] showed that the safety factor decreases with increasing applied load.

3.2. Analysis results for TS specimen

The fatigue behavior of the TS specimen is presented in Figs. 7 and 8. As shown in Figs. 7a–c, increasing tensile stress results in a significant decrease in fatigue life and safety factor, while damage increases for all stress ratios. This behavior is associated with increased stress concentration in the narrow (waist) region of the specimen, where deformation is more pronounced under higher loading conditions. For $R = -0.2$, as illustrated in Fig. 8a, the lowest fatigue life is concentrated in the thin section of the specimen at $\sigma = 483$ MPa. This region acts as the critical location for crack initiation due to geometric stress concentration. As the stress decreases to 241.5 and 120.75 MPa, the affected region becomes smaller and the fatigue life increases. The color transition from low-life regions to high-life regions indicates a reduction in failure-prone areas. For $R = 0.1$, as shown in Fig. 8b, the damage distribution becomes more uniform compared to the $R = -0.2$ case. At $\sigma = 483$ MPa, the failure region is still concentrated in the thin section, but its intensity is reduced. As the stress decreases, the fatigue life increases significantly, and at $\sigma = 120.75$ MPa, high-life regions dominate the specimen. For $R = 0.4$, as illus-

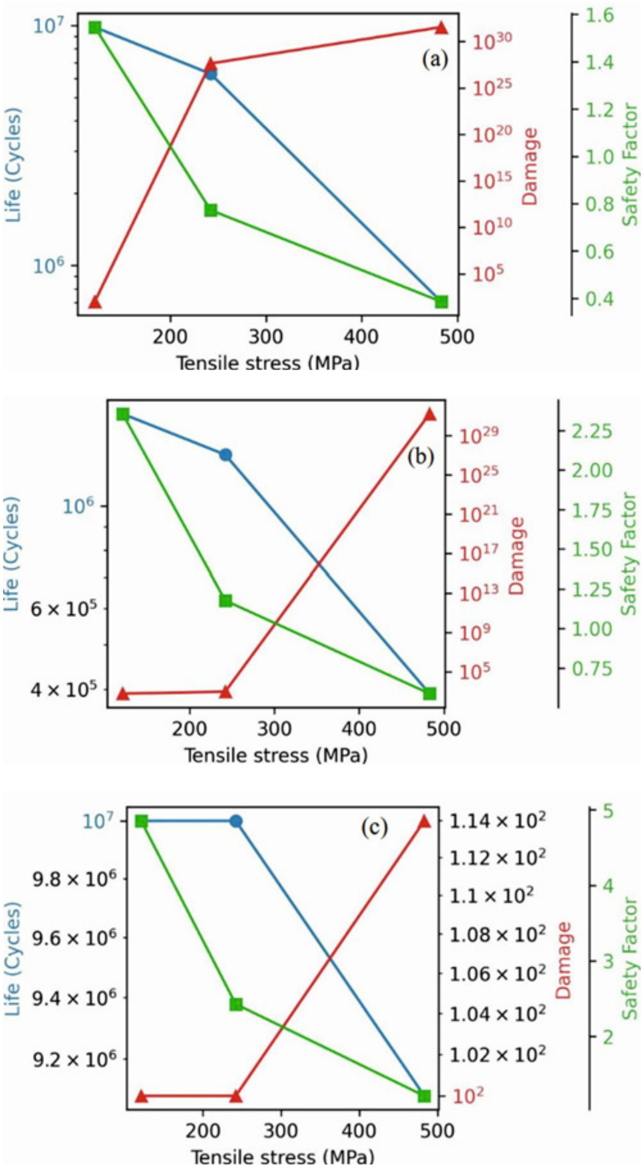

Fig. 7. Variation of parameters for the TS specimen under different stress ratios: (a) $R = -0.2$, (b) $R = 0.1$, and (c) $R = 0.4$.

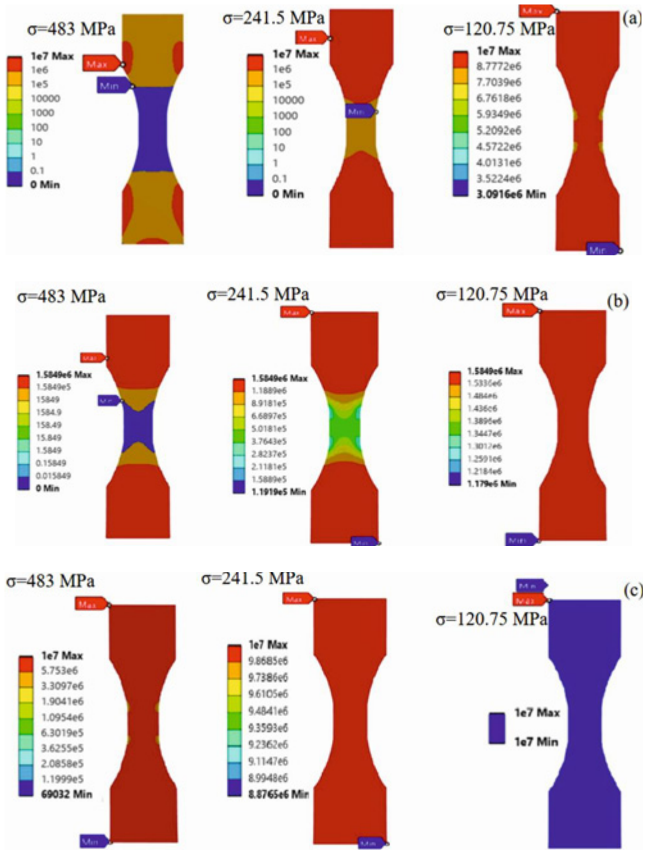

Fig. 8. Variation of deformation for the TS specimen at different stress ratios: (a) $R = -0.2$, (b) $R = 0.1$, and (c) $R = 0.4$.

trated in Fig. 8c, the influence of the positive stress ratio becomes more evident. At lower stress levels, especially at $\sigma = 120.75$ MPa, the specimen exhibits predominantly high-life regions, and the fatigue life can be considered effectively infinite. The contour plots indicate that the failure-prone regions are minimized. These observations indicate that the fatigue behavior of the TS specimen is strongly governed by the geometry of the narrow section. The stress concentration in this region controls crack initiation and propagation. The obtained results are in agreement with previous studies. Liu et al. [38] reported that fatigue failure is dominated by stress concentration regions under high tensile stress conditions.

3.3 Analysis results for SS specimen

The fatigue behavior of the SS specimen is presented in Figs. 9 and 10. As shown in Figs. 9a–c, fatigue life decreases and damage increases with increasing tensile stress for all stress ratios. This behavior is primarily controlled by the notch region, which acts as a stress concentration zone. For $R = -0.2$, as illustrated in Fig. 10a, the lowest fatigue life is concentrated at the notch at $\sigma = 483$ MPa, indicating severe stress concentration. As the applied stress decreases to 241.5 and 120.75 MPa, the fatigue life in the notch region increases significantly. The contour plots show a transition toward higher life regions at lower stress levels. For $R = 0.1$, as shown in Fig. 10b, the fatigue behavior is similar to the $R = -0.2$ case; however, the life distribution becomes more uniform. The notch region still controls the fatigue behavior, but the effect of stress concentration is slightly reduced. For $R = 0.4$, as illustrated in Fig. 10c, the fatigue life increases further, particularly at lower stress levels. The contour plots indicate that high-life regions dominate the specimen, and the damage distribution becomes more uniform. Overall, the fatigue behavior of the SS

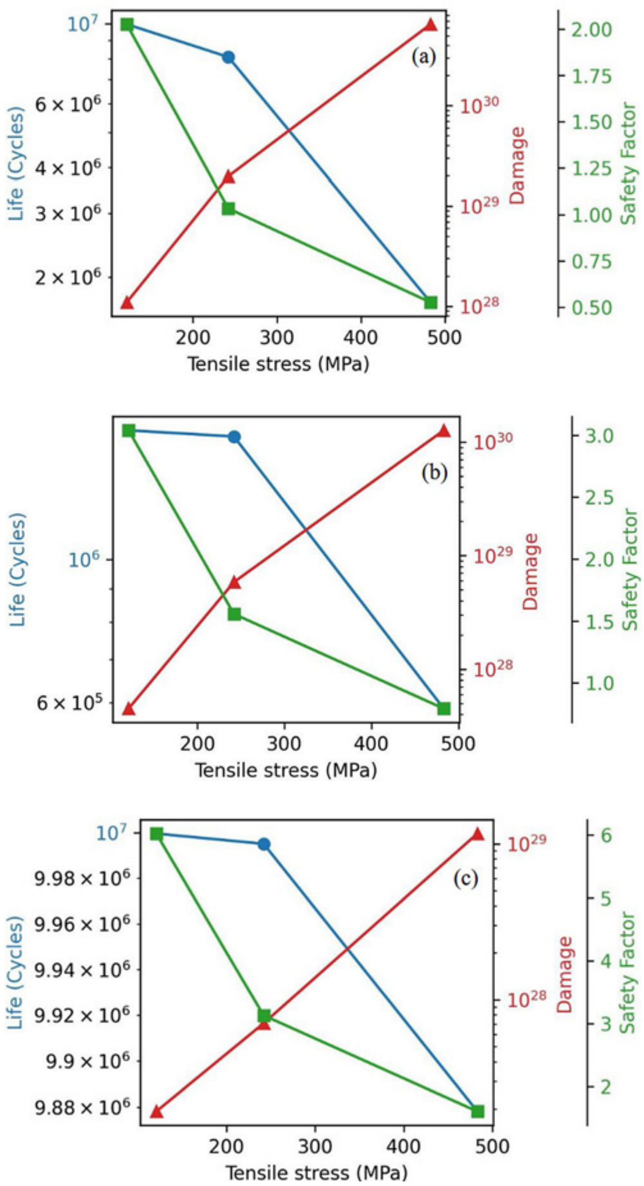

Fig. 9. Variation of parameters for the SS specimen under different stress ratios: (a) $R = -0.2$, (b) $R = 0.1$, and (c) $R = 0.4$.

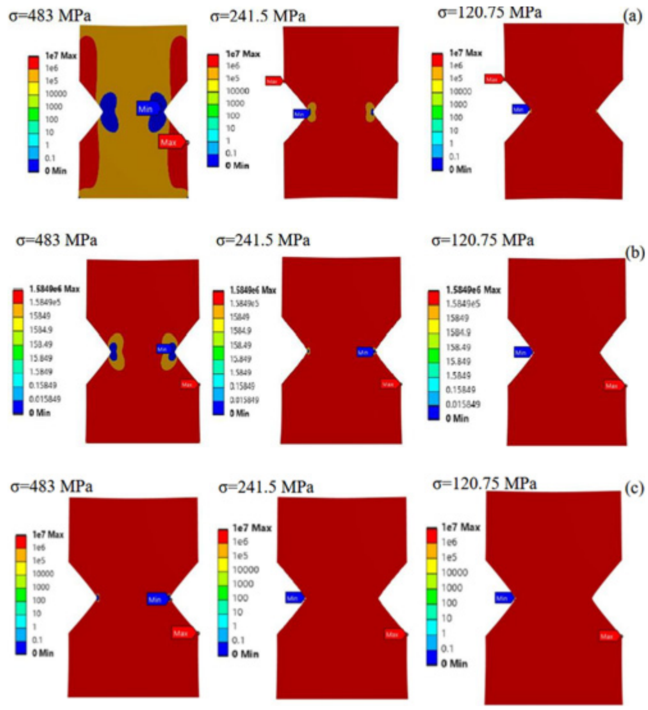

Fig. 10. Variation of deformation for the SS specimen at different stress ratios: (a) $R = -0.2$, (b) $R = 0.1$, and (c) $R = 0.4$.

specimen is governed by the notch geometry, and both stress level and stress ratio significantly influence crack initiation and propagation. These findings are consistent with the study of Roundi and Elgharad [40], who showed numerically that fatigue life increases as the stress ratio approaches positive values.

The overall trends obtained for the OHS, TS, and SS specimens are consistent with the findings reported in the literature. Previous studies have shown that increasing tensile stress accelerates crack initiation and propagation, leading to a significant reduction in fatigue life and an increase in damage accumulation. Similarly, it has been reported that the safety factor decreases with increasing applied stress due to higher loading severity. In addition, stress concentration regions such as holes, notches, and geometrical discontinuities play a dominant role in fatigue failure by acting as primary crack initiation sites. The present results also indicate that the stress ratio has a considerable influence on fatigue behavior, where positive stress ratios can alter damage distribution and fatigue performance depending on specimen geometry. These observations are in agreement with the experimental and numerical findings of Mazlan et al. [37] and Liu et al. [38], who demonstrated that higher stress levels accelerate fatigue damage mechanisms, as well as Evran [39], who reported a decrease in safety factor with increasing applied load. Furthermore, the effect of stress ratio on fatigue life is consistent with the numerical study of Roundi and Elgharad [40], who showed that fatigue performance varies significantly with stress ratio conditions.

The variation of fatigue parameters with respect to stress ratio ($R = -0.2$, 0.1, and 0.4) for different tensile stress levels is presented in Figs. 11–13 for OHS, TS, and SS specimens, respectively. As shown in Figs. 11–13, for all specimen types, fatigue life initially decreases and then increases with increasing R, while the safety factor consistently increases. In contrast, damage generally decreases with increasing R, except for the OHS and TS specimens at $\sigma = 120.75$ MPa, where a non-monotonic behavior is ob-

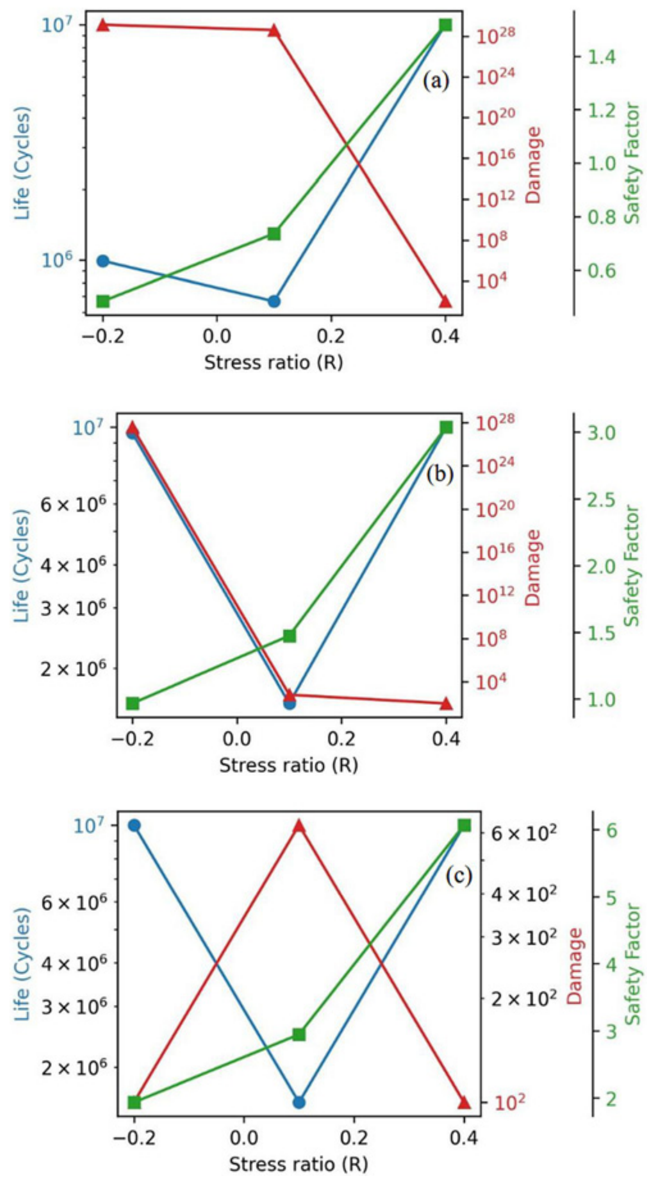

Fig. 11. Variation of fatigue parameters for the OHS specimen at different stress levels: (a) 483 MPa, (b) 241.5 MPa, and (c) 120.75 MPa.

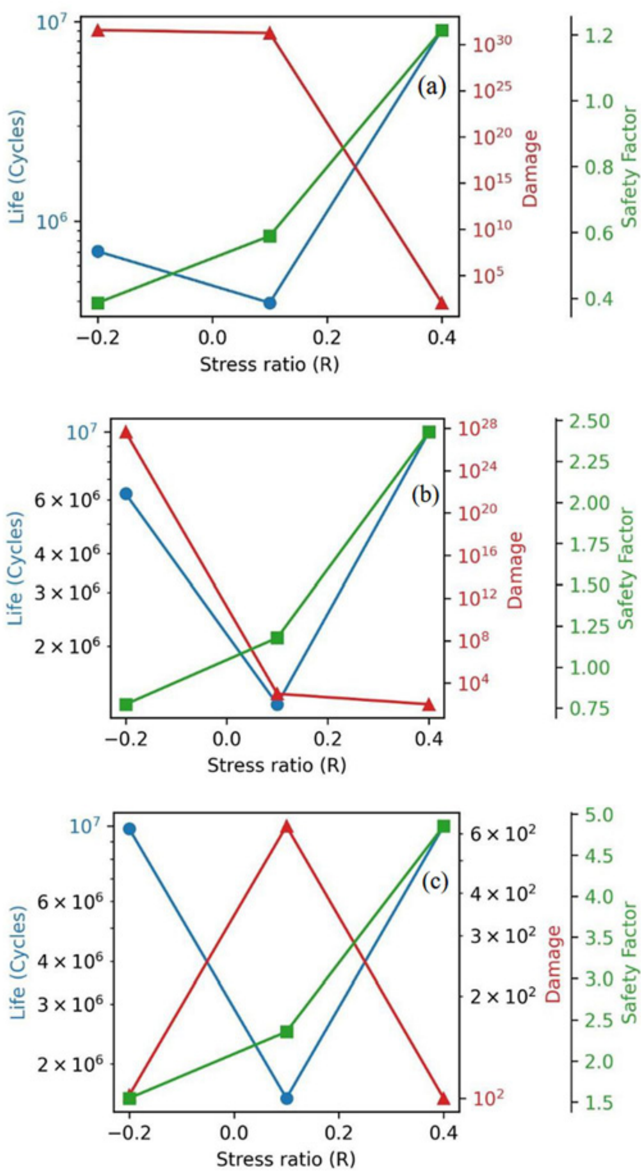

Fig. 12. Variation of fatigue parameters for the TS specimen at different stress levels: (a) 483 MPa, (b) 241.5 MPa, and (c) 120.75 MPa.

served. In these cases, damage first increases and then decreases, forming a triangular trend. This behavior can be explained by considering the effect of stress ratio on the stress range ($\Delta\sigma = \sigma_{\max} - \sigma_{\min}$). As R increases, the minimum stress approaches the maximum stress, leading to a reduction in stress range. A smaller stress range slows down crack propagation, resulting in lower damage accumulation and improved fatigue life. Consequently, the safety factor increases with increasing R. However, when R is negative, crack closure effects occur during cyclic loading. This crack closure reduces the effective stress intensity at the crack tip, thereby slowing down crack growth and increasing fatigue life. As a result, relatively higher life values are observed at both low ($R = -0.2$) and high ($R = 0.4$) stress ratios. At intermediate stress ratios ($R = 0.1$), the cracks tend to remain open during the loading cycle, leading to higher effective stress ranges. This condition accelerates crack propagation and reduces fatigue life. Therefore, the relationship between fatigue life and stress ratio exhibits a nonlinear trend. Damage, which represents the consumed portion of fatigue life, is strongly related to the stress range. As the stress range decreases with increasing R, the rate of damage accumulation also decreases. Additionally, at higher R values, the loading cycle remains predominantly in tension, which reduces the severity of cyclic loading and contributes to improved fatigue perfor-

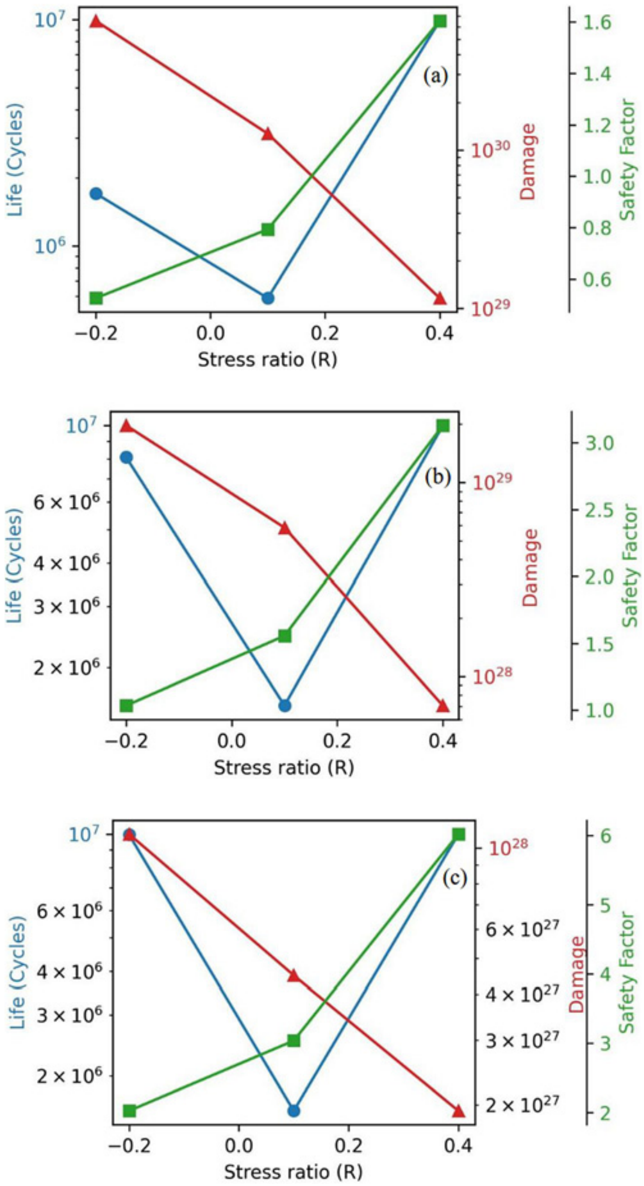

Fig. 13. Variation of fatigue parameters for the SS specimen at different stress levels: (a) 483 MPa, (b) 241.5 MPa, and (c) 120.75 MPa.

mance. Overall, the results clearly indicate that the fatigue response of all specimens is highly sensitive to the stress ratio, and the relationship between R and fatigue life is nonlinear. Similar nonlinear trends between stress ratio and fatigue life have also been reported in the literature by Moers and Dresbach [41].

These results can support researchers in developing more reliable numerical fatigue models and assist engineers in designing safer and more durable structural components, particularly in aerospace applications. Furthermore, the findings of this study may also be applicable to other engineering fields where fatigue-critical metallic structures are used.

4. Conclusion

In this study, the fatigue behavior of 2024-T3 was numerically investigated under different stress ratios ($R = -0.2$, 0.1, and 0.4) and tensile stress levels (483, 241.5, and 120.75 MPa) for three specimen geometries (OHS, TS, and SS). The main findings can be summarized as follows:

– Increasing the tensile stress from 120.75 to 483 MPa resulted in a significant reduction in fatigue life for all specimen types, with life values decreasing by several orders of magnitude, while damage increased substantially.

– Among the specimen geometries, the OHS specimen exhibited the lowest fatigue life due to severe stress concentration around the hole, whereas TS and SS specimens showed relatively higher fatigue resistance.

– The effect of stress ratio on fatigue behavior was found to be nonlinear. Fatigue life decreased at $R = 0.1$ compared to $R = -0.2$, while a noticeable increase in fatigue life was observed at $R = 0.4$, particularly at lower stress levels where the life exceeded 10^6 cycles.

– The safety factor decreased with increasing stress level, while it increased with higher stress ratios, indicating reduced loading severity at higher R values.

– The results demonstrated that fatigue damage initiation and propagation are strongly governed by stress concentration regions such as holes, notches, and geometrical discontinuities.

Overall, the findings clearly indicate that both stress ratio and specimen geometry have a combined and significant influence on fatigue life, damage, and safety factor. Therefore, these parameters must be considered simultaneously for reliable fatigue life prediction and safe design of aluminum alloy structures.

References

[1] J.-J. Yang, S.-Y. Yin, C.-H. Fan, L. Ou, J.-H. Wang, H. Peng, B.-W. Wang, D. Luo, S.-Y. Dong, Z.-Y Zhang, Effect of voltage on structure and properties of 2024 aluminum alloy surface anodized aluminum oxide films, Surf. Coat. Technol. 479 (2024) 130508. https://doi.org/10.1016/j.surfcoat.2024.130508

[2] X. Meng, X. Leng, C. Shan, L. Zhou, J. Zhou, S. Huang, J. Lu, Vibration fatigue performance improvement in 2024-T351 aluminum alloy by ultrasonic-assisted laser shock peening, Int. J. Fatigue 168 (2022) 107471. https://doi.org/10.1016/j.ijfatigue.2022.107471

[3] M. Asmael, B. Safaei, O. Kalaf, Q. Zeeshan, F. Aldakheel, T. Nasir, Z. Yang, Recent developments in tensile properties of friction welding of carbon fiber-reinforced composite: A review, Nanotechnol. Rev. 11 (2022) 1408–1436. https://doi.org/10.1515/ntrev-2022-0083

[4] S. Li, X. Yue, Q. Li, H. Peng, B. Dong, T. Liu, H. Yang, J. Fan, S. Shu, F. Qiu, Q. Jiang, Development

and applications of aluminum alloys for aerospace industry, J. Mater. Res. Technol. 27 (2023) 944–983. https://doi.org/10.1016/j.jmrt.2023.09.274

[5] V. K. Yadav, V. Gaur, I. Singh, Combined effect of residual and mean stresses on fatigue behavior of welded aluminum 2024 alloy, Int. J. Fatigue 155 (2021) 106565. https://doi.org/10.1016/j.ijfatigue.2021.106565

[6] H. B. Younis, K. Kamal, M. F. Sheikh, A. Hamza, Prediction of fatigue crack growth rate in aircraft aluminum alloys using optimized neural networks, Theor. Appl. Fract. Mech. 117 (2021) 103196. https://doi.org/10.1016/j.tafmec.2021.103196

[7] S. Wang, H. Hung, J. Ho, J. Lin, C. Yeh, Improving detection technique for flight recorders of distressed airplanes crashed into ocean, J. Mar. Sci. Technol. 23 (2015) 467–474. https://doi.org/10.6119/jmst-014-1027-1

[8] Y. A. Fageehi, Fatigue crack growth analysis with extended finite element for 3D linear elastic material, Metals 11 (2021) 397. https://doi.org/10.3390/met11030397

[9] A. Li, W. Hu, Z. Zhan, Q. Meng, A novel continuum damage mechanics-based approach for thermal corrosion fatigue life prediction of aluminum alloys, Int. J. Fatigue 163 (2022) 107065. https://doi.org/10.1016/j.ijfatigue.2022.107065

[10] S. Gairola, R. Verma, R. Jayaganthan, Study on fatigue and fracture behavior of Al 2024 alloy through XFEM and stress-life approach, Procedia Struct. Integr. 46 (2023) 182–188. https://doi.org/10.1016/j.prostr.2023.06.031

[11] R. M. Nejad, N. Sina, W. Ma, W. Song, S. Zhu, R. Branco, W. Macek, A. Gholami, Artificial neural network based fatigue life assessment of riveted joints in AA2024 aluminum alloy plates and optimization of riveted joints parameters, Int. J. Fatigue 178 (2023) 107997. https://doi.org/10.1016/j.ijfatigue.2023.107997

[12] S. M. K. Mohammed, R. Mhamdia, A. Albedah, B. A. B. Bouiadjra, B. B. Bouiadjra, F. Benyahia, Fatigue crack growth in aluminum panels repaired with different shapes of single-sided composite patches, Int. J. Adhes. Adhes. 105 (2020) 102781. https://doi.org/10.1016/j.ijadhadh.2020.102781

[13] H. Chen, S. Liu, P. Wang, X. Wang, Z. Liu, F. Aldakheel, Effect of grain structure on fatigue crack propagation behavior of 2024 aluminum alloy under different stress ratios, Mater. Des. 244 (2024) 113117. https://doi.org/10.1016/j.matdes.2024.113117

[14] W. Dai, Z. Liu, C. Li, D. He, D. Jia, Y. Zhang, Z. Tan, Fatigue life of micro-arc oxidation coated AA2024-T3 and AA7075-T6 alloys, Int. J. Fatigue 124 (2019) 493–502. https://doi.org/10.1016/j.ijfatigue.2019.03.028

[15] W. Dai, J. Hao, C. Li, D. He, D. Jia, Y. Zhang, Z. Tan, Residual stress relaxation and duty cycle on high cycle fatigue life of micro-arc oxidation coated AA7075-T6 alloy, Int. J. Fatigue 130 (2019) 105283. https://doi.org/10.1016/j.ijfatigue.2019.105283

[16] M. Borges, P. Lopez-Crespo, F. Antunes, B. Moreno, P. Prates, D. Camas, D. Neto, Fatigue crack propagation analysis in 2024-T351 aluminium alloy using nonlinear parameters, Int. J. Fatigue 153 (2021) 106478. https://doi.org/10.1016/j.ijfatigue.2021.106478

[17] V. Yadav, V. Gaur, I. Singh, Effect of pre-corrosion on crack initiation behavior of friction stir welded aluminum alloy 2024-T3 in high and low cycle fatigue regimes, Int. J. Fatigue 179 (2023) 108037. https://doi.org/10.1016/j.ijfatigue.2023.108037

[18] R. M. Nejad, M. Tohidi, A. J. Darbandi, A. Saber, M. Shariati, Experimental and numerical investigation of fatigue crack growth behavior and optimizing fatigue life of riveted joints in Al-alloy 2024 plates, Theor. Appl. Fract. Mech. 108 (2020) 102669. https://doi.org/10.1016/j.tafmec.2020.102669

[19] R. M. Nejad, F. Berto, M. Tohidi, Fatigue performance prediction of Al-alloy 2024 plates in riveted joint structure, Eng. Fail. Anal. 126 (2021) 105439. https://doi.org/10.1016/j.engfailanal.2021.105439

[20] T. Chakherlou, P. Shahriary, A. Akbari, Experimental and numerical investigation on the fretting fatigue behavior of cold expanded Al-alloy 2024-T3 plates, Eng. Fail. Anal. 123 (2021) 105324. https://doi.org/10.1016/j.engfailanal.2021.105324

[21] G. V. Duncheva, J. T. Maximov, V.P. Dunchev, A. P. Anchev, T. P. Atanasov, Improvement in fatigue performance of 2024-T3 Al alloy via single toroidal roller burnishing, J. Mater. Eng. Perform. 30 (2021) 2256–2266. https://doi.org/10.1007/s11665-021-05535-4

[22] J. T. Maximov, G. V. Duncheva, A. P. Anchev, I. M. Amudjev, New method and tool for increasing fatigue life of a large number of small fastener holes in 2024-T3 Al alloy, J. Braz. Soc. Mech. Sci. Eng. 41 (2019). https://doi.org/10.1007/s40430-019-1709-8

[23] L. Gao, Z. Li, S. Jiang, B. Xie, Dynamic impact behavior and notched fatigue life of GLARE laminates, Compos. Struct. 323 (2023) 117449. https://doi.org/10.1016/j.compstruct.2023.117449

[24] Y. Madhavi, L. R. Krishna, N. Narasaiah, Corrosion-fatigue behavior of micro-arc oxidation coated 6061-T6 Al alloy, Int. J. Fatigue 142 (2020) 105965. https://doi.org/10.1016/j.ijfatigue.2020.105965

[25] K. Ganesan, T. S. Rao, S. K. Rao, Investigating the effect of stress ratio on fatigue crack growth rate behaviour in friction stir welded AA7075-T651 aluminium alloy plates, Int. J. Fatigue 188 (2024) 108527. https://doi.org/10.1016/j.ijfatigue.2024.108527

[26] R. Zhang, W. Zhao, H. Zhang, W. Yang, G. Wang, Y. Dong, C. Ye, Fatigue performance rejuvenation of corroded 7075-T651 aluminum alloy through ultrasonic nanocrystal surface modification, Int. J. Fatigue 153 (2021) 106463. https://doi.org/10.1016/j.ijfatigue.2021.106463

[27] P. You, H. Chen, M. Li, Y. Wu, A simulative study on the effect of friction coefficient and angle on failure behaviors of GLARE subjected to low-velocity impact, Sci. Eng. Compos. Mater. 30 (2023). https://doi.org/10.1515/secm-2022-0194

[28] P. Zamani, A. Jaamialahmadi, L. F. Da Silva, Fatigue life evaluation of Al-GFRP bonded lap joints under four-point bending using strain-life criteria, Int. J. Adhes. Adhes. 122 (2023) 103338. https://doi.org/10.1016/j.ijadhadh.2023.103338

[29] E. Mosayyebi, T. N. Chakherlou, Numerical investigation of patch geometry effect on the fatigue life of aluminum panels containing cracks repaired with

CFRP composite patch using XFEM and CZM approach, Int. J. Adhes. Adhes. 136 (2024) 103882. https://doi.org/10.1016/j.ijadhadh.2024.103882

[30] R. N. Taware, P. S. Shinde, P. Kumar, Fatigue performance of edge cracked aluminium alloy repaired with asymmetrical CFRP patches, Mater. Today Proc. 72 (2022) 1110–1116. https://doi.org/10.1016/j.matpr.2022.09.175

[31] F. Ahmed, R. Mhamdia, S. M. K. Mohammed, F. Benyahia, A. Albedah, B. A. B. Bouiadjra, Analysis of water absorption on the efficiency of bonded composite repair of aluminum alloy panels, Sci. Eng. Compos. Mater. 31 (2024). https://doi.org/10.1515/secm-2022-0235

[32] H. I. Khalaf, R. Al-Sabur, A. Kubit, Ł. Święch, K. Żaba, V. Novák, Experimental investigation of load-bearing capacity in EN AW-2024-T3 aluminum alloy sheets strengthened by SPIF-fabricated stiffening rib, Materials 17 (2024) 1730. https://doi.org/10.3390/ma17081730

[33] ASTM D6484, Standard test method for open-hole compressive strength of polymer matrix composite laminates, ASTM Int., 2014.

[34] ASTM D638, Standard test method for tensile properties of plastics, ASTM Int., 2014.

[35] ASTM D/DM-12, Standard test method for shear properties of composite materials by V-notched rail shear method, ASTM Int., 2012.

[36] M. Kawai, K. Kato, Effects of R-ratio on the off-axis fatigue behavior of unidirectional hybrid GFRP/Al laminates at room temperature, Int. J. Fatigue 28 (2006) 1226–1238. https://doi.org/10.1016/j.ijfatigue.2006.02.020

[37] S. Mazlan, N. Yidris, S. S. R. Koloor, M. Petrů, Experimental and numerical analysis of fatigue life of aluminum 2024-T351 at elevated temperature, Metals 10 (2020) 1581. https://doi.org/10.3390/met10121581

[38] X. Liu, W. Guo, X. Song, Y. Dong, Z. Yang, Experimental study of fatigue failure behavior of aluminum alloy 2024-T351 under multiaxial loading, Eng. Fail. Anal. 164 (2024) 108684. https://doi.org/10.1016/j.engfailanal.2024.108684

[39] S. Evran, Effects of forces and material types on fatigue analysis of beams, CBU J. Sci. 19 (2023) 315–321. https://doi.org/10.18466/cbayarfbe.1324800

[40] W. Roundi, A. Elgharad, Assessment of fatigue behavior and effects of crack growth in aluminium alloys 6082 under various stress ratios, Int. J. Adv. Sci. Eng. Inf. Technol. 6 (2016) 582–587. https://doi.org/10.18517/ijaseit.6.5.842

[41] C. Moers, C. Dresbach, Influence of R-ratio on fatigue of aluminum bonding wires, Metals 13 (2022) 9. https://doi.org/10.3390/met13010009